Topics in Catalysis (2024) 67:698–713
https://doi.org/10.1007/s11244-023-01898-1

ORIGINAL PAPER

Immobilization of Xylanase into Zeolitic Imidazolate Framework-67 (ZIF-67) and Manganese-Doped ZIF-67 (Mn/ZIF-67): A Comparison Study

Büşra Bakar[1] · Gamze Dik[1] · Ahmet Ulu[1] · Burhan Ateş[1]

Accepted: 14 December 2023 / Published online: 31 January 2024

Abstract

It has been discovered that metal–organic frameworks (MOFs) have desirable qualities for the immobilization of enzymes, including a high surface area, significant interior pore volumes, and easily changeable pore size. Herein, the xylanase (Xyl) enzyme was immobilized for the first time to two different carrier supports, zeolitic imidazolate framework-67 (ZIF-67) and manganese-doped ZIF-67 (Mn/ZIF-67) by in situ method. The physicochemical characterizations of MOFs with and without Xyl were performed by FT-IR, XRD, SEM, and EDAX techniques. Xyl@ZIF-67 and Xyl@Mn/ZIF-67 were evaluated in terms of optimum temperature, optimum pH, kinetic parameters, thermal stability, reusability as well as juice clarification and compared with free Xyl. Optimum temperature values were 50 °C for Xyl@ZIF-67 and 70 °C for free Xyl and Xyl@Mn/ZIF-67. Optimum pH values for free Xyl, Xyl@ZIF-67, and Xyl@Mn/ZIF-67 were recorded as 6.0, 8.0, and 7.0, respectively. K_m values for free Xyl, Xyl@ZIF-67, and Xyl@Mn/ZIF-67 were calculated as 3.139, 5.430, and 0.799 mg/mL, respectively, while V_{max} values were calculated as 0.167, 0.226, and 0.062 µmol/min/mL, respectively. The results revealed that in comparison to the free Xyl, Xyl@ZIF-67, and Xyl@Mn/ZIF-67 exhibited more thermal resistance. After incubation at 70 °C for 120 min, the free Xyl remained at 28.7% of the activity, while the Xyl@ZIF-67 and Xyl@Mn/ZIF-67 remained at 85.7% and 40.0%, respectively. Moreover, after eight cycles, the Xyl@ZIF-67 and Xyl@Mn/ZIF-67 retained more than 70% of their initial activity. Further, the transmittance of apple juice was increased from 65.61 to 94.73% and from 77.80 to 84.13%, respectively, when Xyl@ZIF-67 and Xyl@Mn/ZIF-67 were used as biocatalysts. Overall, these findings indicated that the suggested Xyl@ZIF-67 and Xyl@Mn/ZIF-67 have a high potential for juice clarification as an efficient heterogeneous biocatalyst.

✉ Ahmet Ulu
ahmet.ulu@inonu.edu.tr

✉ Burhan Ateş
burhan.ates@inonu.edu.tr

[1] Biochemistry and Biomaterials Research Laboratory, Department of Chemistry, Faculty of Arts and Science, İnönü University, 44280 Malatya, Türkiye

Graphical Abstract

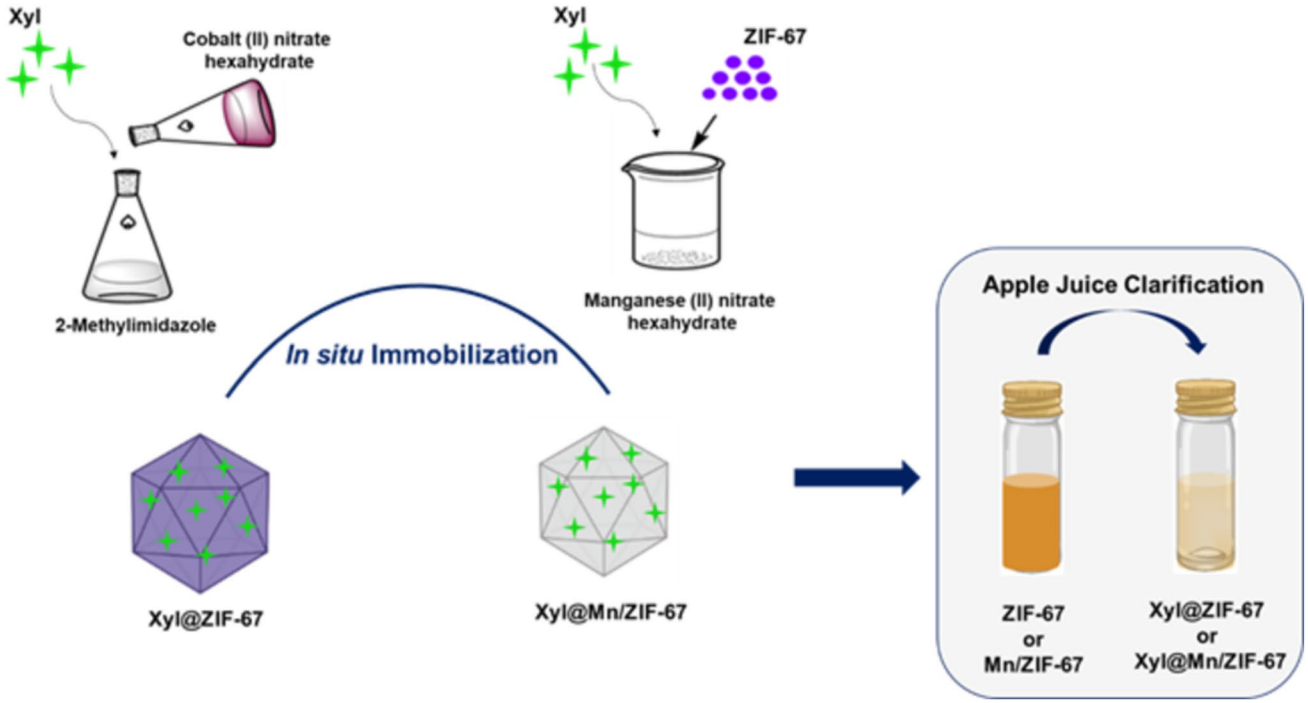

Keywords Zeolitic imidazole framework-67 (ZIF-67) · Manganese · Xylanase · Enzyme immobilization · Juice clarification

1 Introduction

Metal-organic frameworks (MOFs) are formed by the combination of organic ligands and metal ions with coordination bonds. Different metal cations (Cu^{+2}, Zn^{+2}, and Co^{+2}) and organic ligands (imidazolates, carboxylates, phosphonates, and phenolates) have been used in the formation of MOFs. The differentiation of the properties and structures of MOFs depending on the varying organic and inorganic components offers them a wide range of applications. MOFs are gaining increasing popularity in gas storage/separation, catalysis, bioimaging, enzyme immobilization, and drug release applications due to the advantages provided by both organic and inorganic components [1, 2]. In addition, MOFs have superior properties such as crystallographic structure and morphology, high surface area, tunable porosity, and particle size [3, 4].

Zeolitic imidazolate frameworks (ZIFs), a class of MOFs, are formed by bridging transition metal cations by imidazole, 2-methylimidazole, or functionalized imidazole ligands [5]. ZIFs show high porosity and thermal/mechanical stability, tunable surface properties, as well as resistance to alkaline environments and organic solvents, with the advantage of strong metal–nitrogen bonds [6]. They are also porous materials with low toxicity, which can be obtained with fast and easy synthesis steps [7]. Moreover, organic ligands and metal ions with functional groups such as the imidazole group in the ZIFs structure tend to rapidly form stable structures by nucleating around biomolecules [8, 9].

Xylanase enzyme (EC 3.2.1.8, endo-1,4-β-xylan xylanohydrolase, Xyl) catalyzes the hydrolysis of β-1,4 glycosidic bonds of xylose units in the xylan polymer, the main component of hemicelluloses [10]. Xylan is the substrate of the Xyl enzyme and it is the second most abundant carbohydrate in nature after cellulose [11]. The xylose sugar formed as a result of the hydrolysis of xylan and the xylose oligosaccharides formed from this sugar are defined as xylooligosaccharides (XOS) [12, 13]. Xyl enzyme is the key component that makes up XOSs [14]. XOSs act as probiotics, inducing the proliferation of beneficial bacteria while reducing the number of harmful bacteria in the digestive tract [15]. In addition, XOSs have anti-inflammatory agent, anti-cancer, and antioxidant properties [16–18]. Moreover, the Xyl enzyme is of great interest in many industrial areas. For example; it acts as a clarifier in the beverage industry [19], as a feed additive activating the enzymatic degradation of arabinoxylan in the animal feed industry [20], and as a bleaching agent in the paper industry [21]. Considering the increasing demand for natural juice consumption in recent years, the role of the Xyl enzyme in the industry gains importance. Fresh juices are

composed of hemicellulosic components, polysaccharides such as pectin and starch. These polysaccharides tend to precipitate in juices during storage, shortening shelf life and decreasing juice quality [22]. The commercial use of fresh juices in the industry is possible by removing the turbidity caused by polysaccharides. The commercial use of fresh juices in the industry is possible by removing the turbidity caused by polysaccharides [23]. Various physical/chemical methods in juice treatment have not been able to show the desired effect, making it difficult to steer toward the storage and commercial market. The removal of turbidity as a result of enzymatic processes gains importance with the low toxicity, high efficiency, selectivity, and mild reaction conditions of the enzymes. The sensitivity and decreasing stability of enzymes to industrial conditions limit the adaptation process of the Xyl enzyme, which has a wide industrial spectrum and causes high costs due to difficulties in storage and reusability. In addition, the inability to separate the soluble enzyme in the reaction medium, product contamination, high temperature, pH, and the presence of inhibitors are other factors limiting the application [19]. Enzyme immobilization is a method that offers advantages such as increased enzyme stability, resistance to environmental conditions, and improved application cost with the effect of the selected appropriate carrier support. The tendency of many carriers supports used in the immobilization process to be in amorphous structure and not having sufficient flexibility causes limitations in practice [24, 25]. Xyl enzyme was immobilized to many carriers supports divided into organic, inorganic, and composite materials such as chitosan beads [26], copper-based MOF [10], hydroxyapatite nanoparticles modified with metal ions [27], nanoflower [28], silica encapsulated magnetic nanoparticles [19], and superparamagnetic graphene oxide nanosheets [11]. However, there is very little investigation regarding the optimization of Xyl immobilization using MOF as support. In this view of the background, there is a much greater need for innovative materials and strategies, and researchers have focused more on this topic in recent years.

We have witnessed in previous studies that manganese ions (Mn^{2+}) improve the catalytic activity of Xyl [29, 30]. Therefore, the aim of the current study was to realize the enhancement of Xyl catalytic performance via the addition of manganese (Mn) ions and to develop a promising perspective for the fabrication of enzyme carrier materials. Thanks to our approach, this work may offer a novel way to improve the activity of enzymatic reactions for laboratory or even industrial use. Herein, the selection of ZIF-67 supports for immobilization of the Xyl was dictated by their properties, such as porosity and thermal/mechanical stability, which can increase immobilization efficiency and stabilize the structures of the immobilized enzymes. The zeolitic imidazolate framework-67 (ZIF-67) and manganese-doped ZIF-67 (Mn/ZIF-67) were synthesized and employed as the support for in situ immobilization of Xyl. The characterization procedure of the ZIF-67, Mn/ZIF-67, Xyl@ZIF-67, and Xyl@Mn/ZIF-67 was determined using ultraviolet-visible spectroscopy (UV–Vis), Fourier transforms infrared spectroscopy (FT-IR), X-ray diffraction (XRD), scanning electron microscopy (SEM), and energy dispersive X-ray spectroscopy (EDAX). In addition, optimal conditions (temperature and pH) of free Xyl, Xyl@ZIF-67, and Xyl@Mn/ZIF-67 were defined and the reusability, thermal stability, and thermodynamic parameters for thermal denaturation were conducted. Further, kinetic parameters (V_{max} and K_m) were calculated and analyzed in detail. Most importantly, the potential of the Xyl@ZIF-67 and Xyl@Mn/ZIF-67 was examined to improve the clarification of apple juice.

2 Materials and methods

2.1 Materials

Xyl enzyme (≥ 2500 units/g, recombinant, expressed in *Aspergillus oryzae*), trichloroacetic acid (TCA, ≥ 99.0%), cobalt(II) nitrate hexahydrate ($Co(NO_3)_2{\cdot}6H_2O$, ≥ 98%), manganese(II) nitrate tetrahydrate ($Mn(NO_3)_2{\cdot}4H_2O$, ≥ 97.0%), xylose (≥ 98%), and 2-methylimidazole (2-MI, 99%) were purchased from Sigma-Aldrich (St. Louis MO, USA). 3,5-dinitrosalicylic acid (DNS, 97%) was obtained from Alfa Aesar (Ward Hill, MA). Xylan from beechwood (≥ 95%) was supplied by Carl Roth (Karlsruhe, Germany). Unless otherwise stated, other chemicals were of analytical purity and were used without further purification. Ultrapure water (Millipore Direct-Q3 System) was used to prepare aqueous solutions.

2.2 Synthesis Procedure of ZIF-67 and Mn/ZIF-67

The synthesis of ZIF-67 was carried out according to the method applied by Guo et al. [31]. In brief, 10 mmol (2.910 g) of $Co(NO_3)_2{\cdot}6H_2O$ and 40 mmol (3.284 g) of 2-MI were each dissolved separately in 200 mL of methanol. Then, $Co(NO_3)_2{\cdot}6H_2O$ solution was added to 2-MI solution and the mixture solution was stirred at room temperature for 30 min. Then, the mixture solution was at room temperature for 24 h. The purple precipitates formed were separated from the mixture by centrifugation at 5000 rpm for 10 min. The crystals were then washed several times with methanol and finally dried under a vacuum at 60 °C. The synthesis of Mn/ZIF-67 was carried out with minor modifications to the method applied by Lourenço et al. [32]. Briefly, 400 mg of $Mn(NO_3)_2{\cdot}4H_2O$ was dissolved in 100 mL of methanol. Then, 50 mg of ZIF-67 was added into $Mn(NO_3)_2{\cdot}4H_2O$ solution, and the final mixture was stirred for 30 min at room

temperature. After waiting for 24 h, the mixture was centrifuged at 5000 rpm for 10 min. Finally, the resulting product was washed several times with methanol and dried under a vacuum at 60 °C. Figure 1 shows a schematic illustration of the synthesis steps for ZIF-67 and Mn/ZIF-67.

2.3 Xyl Immobilization

The immobilization of the Xyl was carried out during the synthesis of ZIF-67 and Mn/ZIF-67 by in situ (adding an enzyme to synthesis in one step) method (Fig. 2). In the

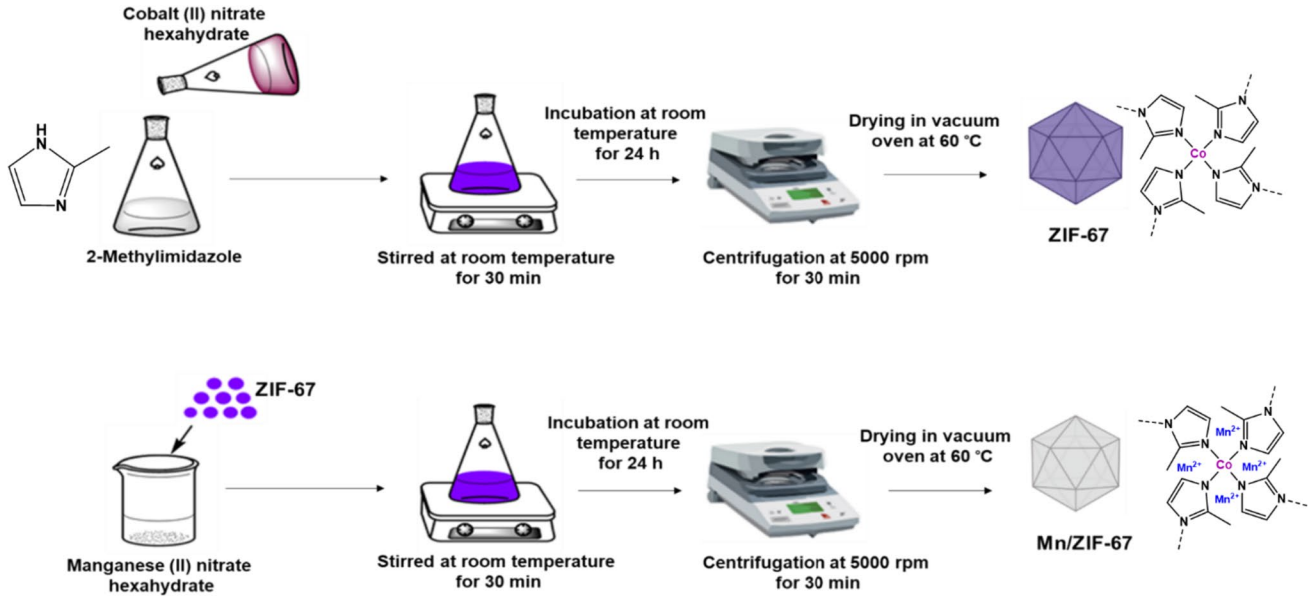

Fig. 1 A schematic illustration of the synthesis steps for ZIF-67 and Mn/ZIF-67

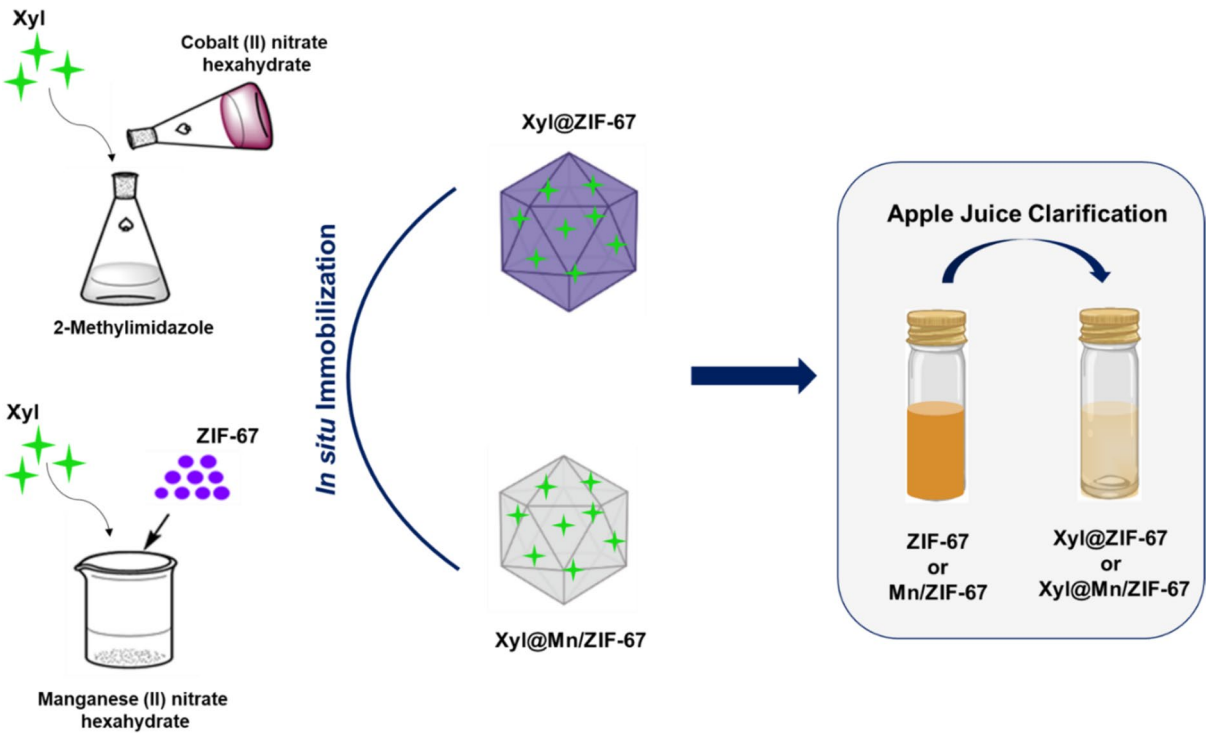

Fig. 2 Schemes of the one-step in situ immobilization of Xyl@ZIF-67 and Xyl@Mn/ZIF-67 to juice clarification

ZIF-67 synthesis step, 20 U/mL of Xyl enzyme solution prepared with sodium acetate buffer (50 mM, pH 6.0) was added to $Co(NO_3)_2{\cdot}6H_2O$ solution. The mixture was then added to 2-MI. The aforementioned synthesis steps were continued and Xyl@ZIF-67 was synthesized. In the Mn/ZIF-67 synthesis step, 20 U/mL of Xyl enzyme solution prepared with sodium acetate buffer (50 mM, pH 6.0) was added to the $Mn(NO_3)_2{\cdot}4H_2O$ solution. By continuing the aforementioned synthesis steps, the Xyl@Mn/ZIF-67 was synthesized. Finally, Xyl@ZIF-67 and Xyl@Mn/ZIF-67 were gathered by centrifugation at 5000 rpm for 5 min. The drying process of both immobilized enzymes was carried out at 37 °C.

2.4 Determination of Xyl Activity

Xyl activity was determined by measuring the amount of reducing xylose sugar released by xylan hydrolysis using DNS reagent [33]. To prepare the DNS reagent, 1 g of 3,5-dinitrosalicylic acid was first dissolved in 2 N 20 mL of NaOH. Then, 5 g of sodium-potassium tartrate was added to the DNS solution and the final volume was completed to 100 mL with distilled water. For the measurement of Xyl activity, a 1% (w/v) xylan solution was prepared using sodium acetate buffer (50 mM, pH 6). 2 mg of Xyl@ZIF-67 and Xyl@Mn/ZIF-67 and 20 µL (20 U/mL) of free Xyl were added to 1 mL of 1% (w/v) xylan solution. Free Xyl, Xyl@ZIF-67, and Xyl@Mn/ZIF-67 were then incubated in a water bath at 60 °C for 10 min. Xyl@ZIF-67 and Xyl@Mn/ZIF-67 were centrifuged at 5000 rpm for 5 min at 4 °C. 1.5 mL of DNS reagent was added to all samples to terminate the catalytic activity. After that, the tubes containing enzyme samples were kept in boiling water for 5 min and then cooled at room temperature. The absorbance of the resulting reducing sugar was measured at 540 nm using a microplate reader controlled by the Gen5 Data Analysis software (BioTek Instruments, Inc., Winooski, VT, USA). The produced xylose equivalents were calculated via a xylose standard curve. One unit (IU) of Xyl activity was determined as the amount of enzyme that produces 1 µmol of xylose per minute. All measurements were made in triplicate and results are given as mean ± standard deviation.

2.5 Determination of Optimum Temperature and pH

The activity of free Xyl, Xyl@ZIF-67, and Xyl@Mn/ZIF-67 was evaluated at varying temperatures and pHs, according to the standard assay condition. The temperature varied from 30 to 80 °C, whereas the pH ranged from pH 4.0 to 10.0. The enzyme activities at optimum conditions were considered 100% and the results were presented as relative activity. Moreover, the activation energy (E_a) of the free Xyl, Xyl@ZIF-67, and Xyl@Mn/ZIF-67 was calculated from the slope of the Arrhenius plot according to the following Eq. 1. The slope was determined by plotting the graph of the log of relative activity versus 1000/T [K] [34].

$$\text{Slope} = -\frac{\text{Ea}}{\text{R}} \tag{1}$$

The temperature coefficient value (Q_{10}) for optimal temperatures of free Xyl, Xyl@ZIF-67, and Xyl@Mn/ZIF-67 was calculated via the following Eq. 2 [35].

$$Q_{10} = \text{antilog}\left(\text{E}_\text{a}10/\text{RT}\right) \tag{2}$$

where E_a is the activation energy (kJ/mol), R is the gas constant (8.314 J/mol/K), and T is the absolute temperature (K).

2.6 Determination of Kinetic Parameters

To estimate the kinetic parameters, the activity of free Xyl, Xyl@ZIF-67, and Xyl@Mn/ZIF-67 was measured by preparing xylan solutions at different concentrations (0.05–4.0 mg/mL). The apparent maximum velocity (V_{max}) and Michaelis–Menten constant (K_m) were calculated with the Lineweaver Burk plot obtained from the Michaelis–Menten equation.

2.7 Investigation of Thermal Stability

To investigate the thermal stability of free Xyl, Xyl@ZIF-67, and Xyl@Mn/ZIF-67, their activities were measured at different incubation times (15, 30, 45, 60, 90, and 120 min) at 50 °C, 60 °C, and 70 °C. At the end of each incubation, the samples were subsequently cooled to room temperature, and the residual activity was measured at the optimum temperatures using the routine Xyl activity assay. The enzyme activity at 15 min was considered 100% and the results were given as relative activity.

2.8 Determination of Reusability

Reusability is the most important advantage of immobilized enzymes over their free counterparts, which reduces the cost in industrial applications. The reusability of Xyl@ZIF-67 and Xyl@Mn/ZIF-67 was achieved by measuring activity under optimum conditions. After the first activity measurement, centrifugation was performed to separate the supernatant and immobilized enzymes. Afterward, the activity was measured in the supernatant, and the fresh substrate solution was added to the separated immobilized enzymes. This catalytic cycle was repeated 8 times. The initial activity was considered as 100% and the subsequent activities were presented as relative activity.

2.9 Application of Immobilized Enzymes in Apple Juice Clarification

The effects of Xyl@ZIF-67 and Xyl@Mn/ZIF-67 on juice clarification were investigated using apple juice. Fresh apple (*Malus domestica*) fruits were purchased from a local market. The clarification procedure was performed according to previous works [36, 37]. Purchased apples were weighed before extracting the juice. The apples were washed with tap water, peeled, and cut into small pieces. Then the pieces were shredded with the help of a household blender and filtered through cheesecloth to separate from the pulp. The juice yield was calculated by measuring the weight of the juice obtained according to Eq. 3 [38]. The fresh apple juice was kept at 90 °C for a few minutes for pasteurization. For clarification, the pHs of the juices were adjusted to pH 8.0 and 7.0, which were the optimum pHs of Xyl@ZIF-67 and Xyl@Mn/ZIF-67, respectively. The centrifugation was carried out at 10,000 rpm for 5 min to ensure complete separation of the apple juice from the pulp. Then, 2 mL of apple juice was added to 5 mg of ZIF-67, Mn/ZIF-67, Xyl@ZIF-67, and Xyl@Mn/ZIF-67. The clarification process was carried out by incubating Xyl@ZIF-67 and Xyl@Mn/ZIF-67 at optimum temperatures for 60 min. After incubation, juice clarity was determined by measuring the percent transmittance (%T) at 660 nm using a spectrophotometer. Furthermore, the change in the amount of reduced sugar after clarification was determined using the DNS method [33]. ZIF-67 and Mn/ZIF-67 constructs were used as controls of immobilized enzymes.

$$\text{Juice yield}(\%) = \frac{\text{weight of juice}}{\text{weight of fruit}} \times 100 \quad (3)$$

2.10 Characterization

FT-IR spectra were monitored on a Perkin Elmer Spectrum 100 spectrometer (PerkinElmer, Waltham, MA, USA) fitted with a Universal Attenuated Total Reflectance (ATR) in a wavelength range of 400–4000 cm^{-1}. XRD patterns were determined by powder X-ray diffractometer (Rigaku RadB-DMAX II) at 10−80° in the 2θ range. Surface morphology at various magnifications was investigated by SEM (EVO 40-LEO, LEO Ltd., Cambridge, UK). The elemental composition was determined via an EDAX detector (model 125 eV; Bruker AXS, Berlin, Germany). The UV–Vis absorption spectra were obtained with Shimadzu's UV-1601 UV–Vis spectrophotometer. The absorbance measurements were performed on an Eon Microplate Reader controlled by Gen5 2.0 Data Analysis Software (BioTek Instruments, Inc., Winooski, VT, USA).

3 Results and Discussion

3.1 Sample Characterization

The FT-IR spectra of the molecular structures of 2-MI, ZIF-67, Mn/ZIF-67, Xyl, Xyl@ZIF-67, and Xyl@Mn/ZIF-67 are shown in Fig. 3. Besides, Table 1 shows comparative table of wavenumber assignments. The broad and strong absorption band observed in the range of 2200–3200 cm^{-1} in the spectrum of 2-MI can be attributed to the bond vibration between pyrrole and pyridinic nitrogen (N–H···N). The absorption band at 1835 cm^{-1} can be attributed to the N–H stretching vibration. Depending on the skeletal vibration of the imidazole ring, absorption peaks are observed at 1832, 1591,

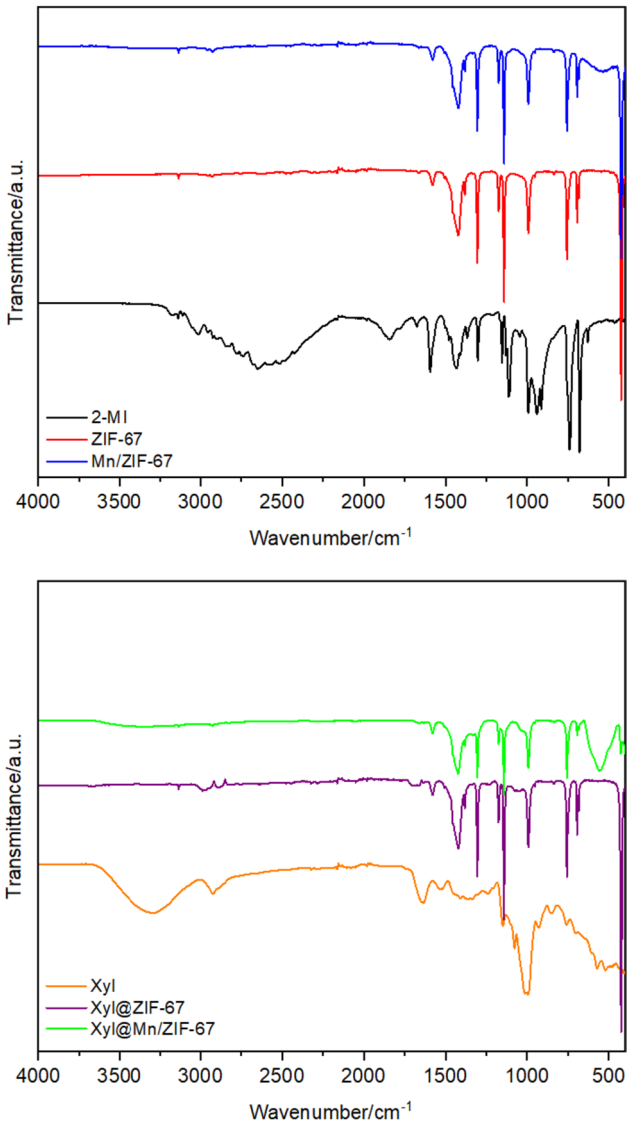

Fig. 3 FT-IR spectra of 2-MI, Xyl, ZIF-67, Mn/ZIF-67, Xyl@ZIF-67, and Xyl@Mn/ZIF-67

Table 1 Comparative table of wavenumber assignments of FT-IR for 2-MI, Xyl, ZIF-67, Mn/ZIF-67, Xyl@ZIF-67, and Xyl@Mn/ZIF-67

Wavenumber (cm^{-1})						
Assigned structural units	2-MI	Xyl	ZIF-67	Mn/ZIF-67	Xyl@ZIF-67	Xyl@Mn/ZIF-67
O–H stretching	–	3296	–	–	–	–
N–H stretching	1835	–	1832	–	–	–
CH asymmetric stretching	1591−1427	2922	–	–	–	–
CH sp^3 (aromatic)	3136−2923	–	3136−2923	3136−2923	3136−2923	–
Amide I band	–	1630	–	–	1670	1670
Amide II band	–	1520	–	–	1575	1575
C–N stretching	1142	–	1142	1142	1142	1142
C–N bending	992	–	992	992	992	992
C=N out-of-plane stretching	756–1577	–	756–1591	756–1577	756–1577	756–1577
Co–N stretching	–	–	424	426	424	426
Mn–N stretching	–	–	–	546	–	546

and 1427 cm^{-1}. Specific absorption peaks are observed at 680–740 and 935–1300 cm^{-1} due to the out-of-plane and in-plane vibration of 2-MI. When compared with 2-MI, the disappearance of the broadband at 2200–3200 cm^{-1} in the ZIF-67 and Mn/ZIF-67 spectra, as well as the absorption band observed at 1832 and 1591 cm^{-1}, explains the formation of ZIF structures [39]. The existence of the bond between the 2-MI ligand supporting the ZIF-67 structure and the metal ions can be attributed to the Co–N stretching vibration band seen at 424 cm^{-1}. The presence of the Co–N bond is also seen in ZIF-67, Mn/ZIF-67, and Xyl@ZIF-67 structures. While the C–N bending vibration occurs at 992 cm^{-1}, the stretching vibration from C–N shows an absorption band at 1142 cm^{-1} [40]. Absorption peaks are observed at 756 and 1577 cm^{-1} due to the C=N out-of-plane stretching vibration of 2-MI. C–N bending and stretching vibrations show their presence with peaks of 992 and 1142 cm^{-1}, respectively. In addition, the absorption bands of ZIF-67, Mn/ZIF-67, and Xyl@ZIF-67 at 3136 and 2923 cm^{-1} are coupled to the stretching vibration of the C–H sp^3 aromatic ring of 2-MI and the C–H sp^2 aliphatic hydrocarbon chain [41]. Absorption bands at 426 and 546 cm^{-1} in Mn/ZIF-67 structure are dependent on Co–N and Mn–N stretching vibration. This is an indication that Mn^{+2} is included in the ZIF-67 structure. The characteristic absorption bands of Xyl at 1630 and 1520 cm^{-1} are attributed to the C=O amide I and N–H amide II bond. In addition, 3296 cm^{-1} O–H stretching vibration and 2922 cm^{-1} C–H asymmetric stretch absorption band were observed [42]. The amide I and amide II absorption bands at 1575–1670 cm^{-1} in the FT-IR spectrum of Xyl@ZIF-67 prove that the enzyme is immobilized to ZIF-67. While the 426 cm^{-1} Co–N stretch in Xyl@Mn/ZIF-67 belongs to ZIF-67, it is seen that the Mn–N absorption band forms a sharp peak compared to Mn/ZIF-67 at 545 cm^{-1}. Therefore, all of these results verified the successful immobilization of Xyl into the ZIF-67 and Mn/ZIF-67 supports.

Figure 4 shows XRD patterns of ZIF-67, Mn/ZIF-67, Xyl@ZIF-67, and Xyl@Mn/ZIF-67. For ZIF-67 structures, the characteristic diffraction peaks appeared at 2θ = 7.32°, 10.38°, 12.7°, 14.7°, 16.42°, 17.94°, 22.08°, 24.44°, 26.66°, and 29.62°. Consistency of this XRD pattern with previous reports indicated the successful formation of the ZIF-67 crystal structure [43]. It was seen that new peaks did not appear in Mn/ZIF-67 and Xyl@ZIF-67 structures, but the intensity of the existing peaks decreases. In addition, it was observed that the crystallinity of Mn/ZIF-67 deteriorated after enzyme immobilization. The reason for this is that the enzyme occupies some parts of the Mn/ZIF-67 structure [25, 44].

UV–Vis spectra of ZIF-67, Mn/ZIF-67, Xyl@ZIF-67, and Xyl@Mn/ZIF-67 are given in Fig. 5. For the spectrum

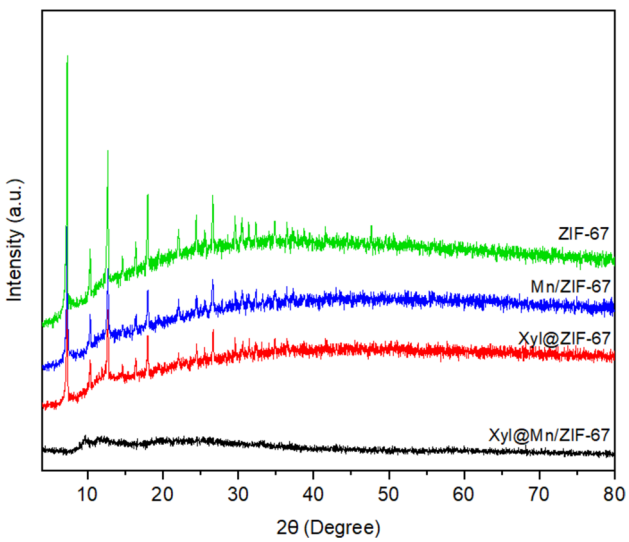

Fig. 4 XRD patterns of ZIF-67, Mn/ZIF-67, Xyl@ZIF-67, and Xyl@Mn/ZIF-67

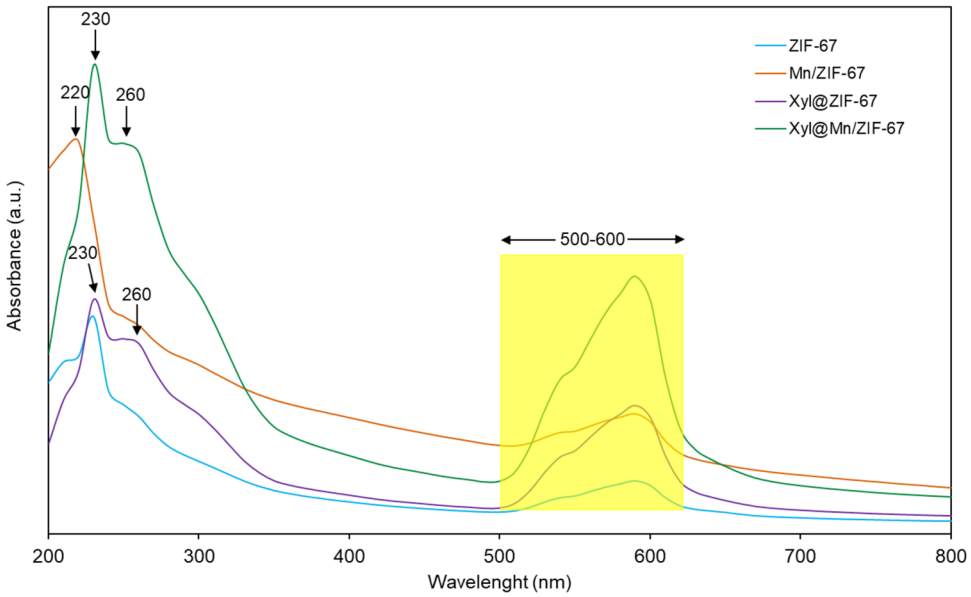

Fig. 5 UV–Vis spectra of ZIF-67, Mn/ZIF-67, Xyl@ZIF-67, and Xyl@Mn/ZIF-67

of ZIF-67, it showed a sharp peak at 230 nm and a wider absorption band between 500 and 600 nm. The band at 230 nm confirmed the existence of metal–ligand charge transfer between Co and oxygen (O) [45]. Broadband indicated the presence of tetrahedral and octahedral coordinated cobalt (Co) ions of the ZIF-67 structure [46]. Mn/ZIF-67 exhibited a similar spectrum to ZIF-67. However, the sharp band at 230 nm shifted to 220 nm due to the doping of Mn ions. Xyl@ZIF-67 and Xyl@Mn/ZIF-67 had characteristic absorption bands of pure materials. However, a new peak appeared at 260 nm due to the presence of the Xyl enzyme [47]. Overall, the observed changes in the UV–Vis spectra implied the immobilization of Xyl.

In Fig. 6, the morphological features of ZIF-67, Mn/ZIF-67, Xyl@ZIF-67, and Xyl@Mn/ZIF-67 were investigated by SEM images. SEM images show the characteristic regular rhombic dodecahedron crystal morphology of ZIF-67. This confirms previous literature studies, showing that ZIF-67 constructs were successfully synthesized [2, 48]. In addition, the fact that the surface morphologies of ZIF-67 and Xyl@ZIF-67 are similar and that enzyme immobilization does not cause a change in the crystal structure supports similar studies [49, 50]. Doping Mn to ZIF-67 structures caused a wide growth orientation and increased crystal size as a result of deprotonation of the organic binder, resulting in slight changes in the crystal morphology of Mn/ZIF-67 [51]. In contrast to Xyl@ZIF-67, enzyme immobilization caused changes in Mn/ZIF-67 structures. Similar to our images, Xu et al. encapsulated N-acetylhexoamine 1-Kinase (NahK) into Mn-doped metal-organic material (Mn-Zn-MOM) [44]. They observed that Mn-ZIF-90 changed in rhombohedral dodecahedral crystal structure and NahK@Mn-Zn-MOM structure changed as dispersed ellipsoid crystals.

The presence of Xyl in ZIF-67 constructs was confirmed by EDAX analysis before and after immobilization. The EDAX patterns of ZIF-67, Mn/ZIF-67, Xyl@ZIF-67, and Xyl@Mn/ZIF-67 are shown in Fig. 7. The presence of carbon (C), nitrogen (N), oxygen (O), and Co elements confirmed the successful synthesis of ZIF-67. Additionally, the presence of the Mn element observed in EDAX patterns of Mn/ZIF-67 supported the successful doping of Mn into the ZIF-67 structure. After Xyl immobilization, a sulfur (S) element peak appeared in the EDAX pattern of Xyl@ZIF-67 and Xyl@ZIF-67, which was attributed to the presence of the enzyme. The presence of the S peak was due to the amino acid residues in the protein structure of Xyl [52]. These outcomes revealed that the Xyl enzyme was immobilized to ZIF-67 and Mn/ZIF-67 structures.

3.2 Biochemical Evaluation of Free and Immobilized Enzyme

3.2.1 Effect of Temperature and pH on the Activity

The relative activities of free Xyl, Xyl@ZIF-67, and Xyl@Mn/ZIF-67 at different temperatures ranging from 30 to 80 °C are shown in Fig. 8A. The free Xyl and Xyl@Mn/ZIF-67 showed the highest activity at 70 °C while Xyl@ZIF-67 had the highest activity at 50 °C. It is well known that after immobilization the optimum temperature can change or remain the same. However, the activity of free Xyl, Xyl@ZIF-67, and Xyl@Mn/ZIF-67 decreased at high temperatures without exception. For instance, at 80 °C, the relative enzyme activity of the free Xyl was 60%, whereas Xyl@ZIF-67 and Xyl@Mn/ZIF-67 retained 65.8% and 72.4%, respectively. The results clearly revealed that the immobilization

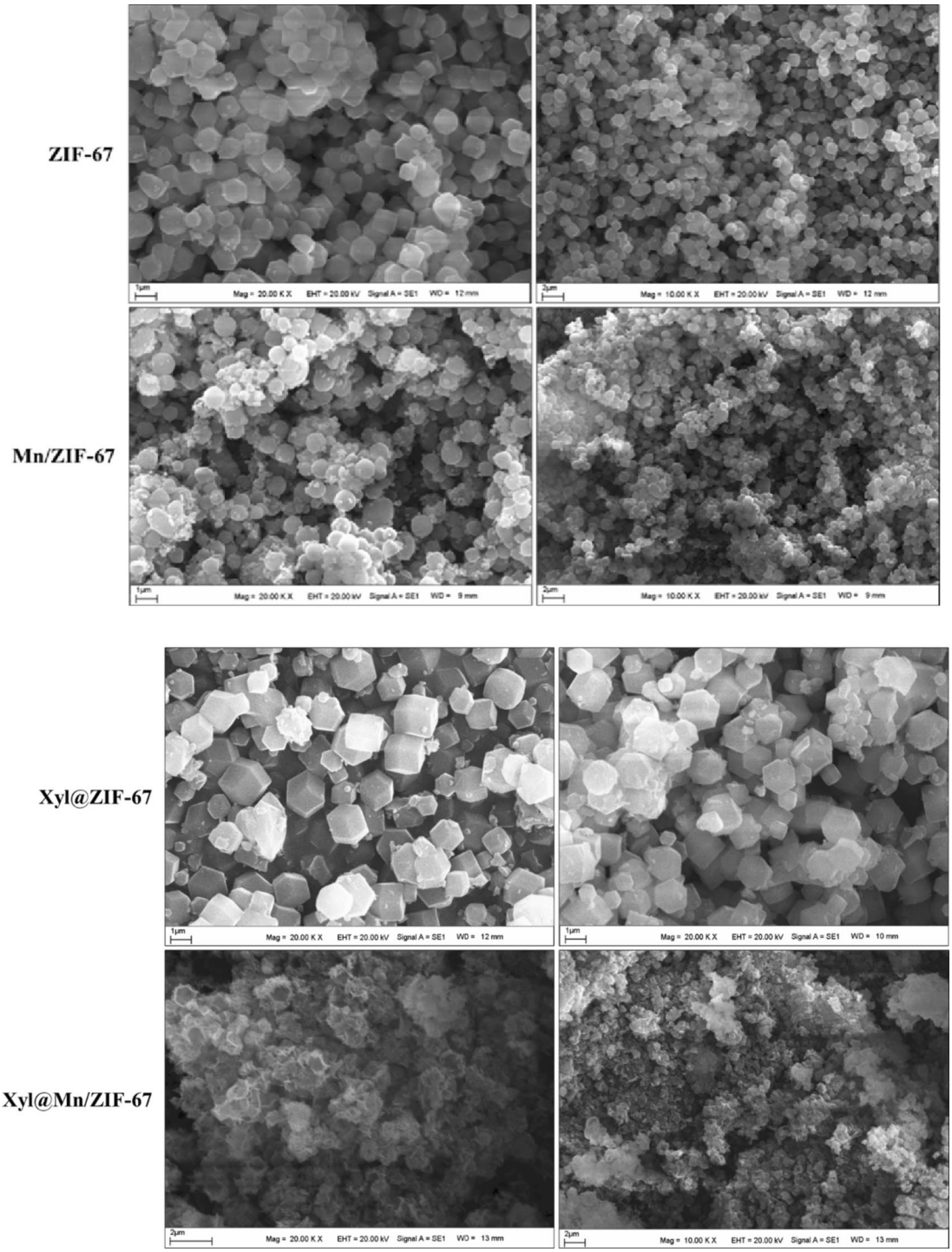

Fig. 6 SEM images of ZIF-67, Mn/ZIF-67, Xyl@ZIF-67, and Xyl@Mn/ZIF-67 at different magnifications

process of Xyl prevented conformation transition at high temperatures and increase the thermostability of Xyl. The thermostability can be attributed to the interactions that occur between the support and the enzyme biomolecules [53]. Moreover, it should be noted that the results show the significantly higher relative activity of Xyl@Mn/ZIF-67 compared with Xyl@ZIF-67, at 70 and 80 °C. The main reason for this may be better stabilization of the tertiary structure of Xyl after doping of Mn ions with ZIF-67.

The relative activities of free Xyl and Xyl@ZIF-67, Xyl@Mn/ZIF-67 at pH values varying between pH 4.0–10.0 are given in Fig. 8B. The free Xyl showed its highest activity at

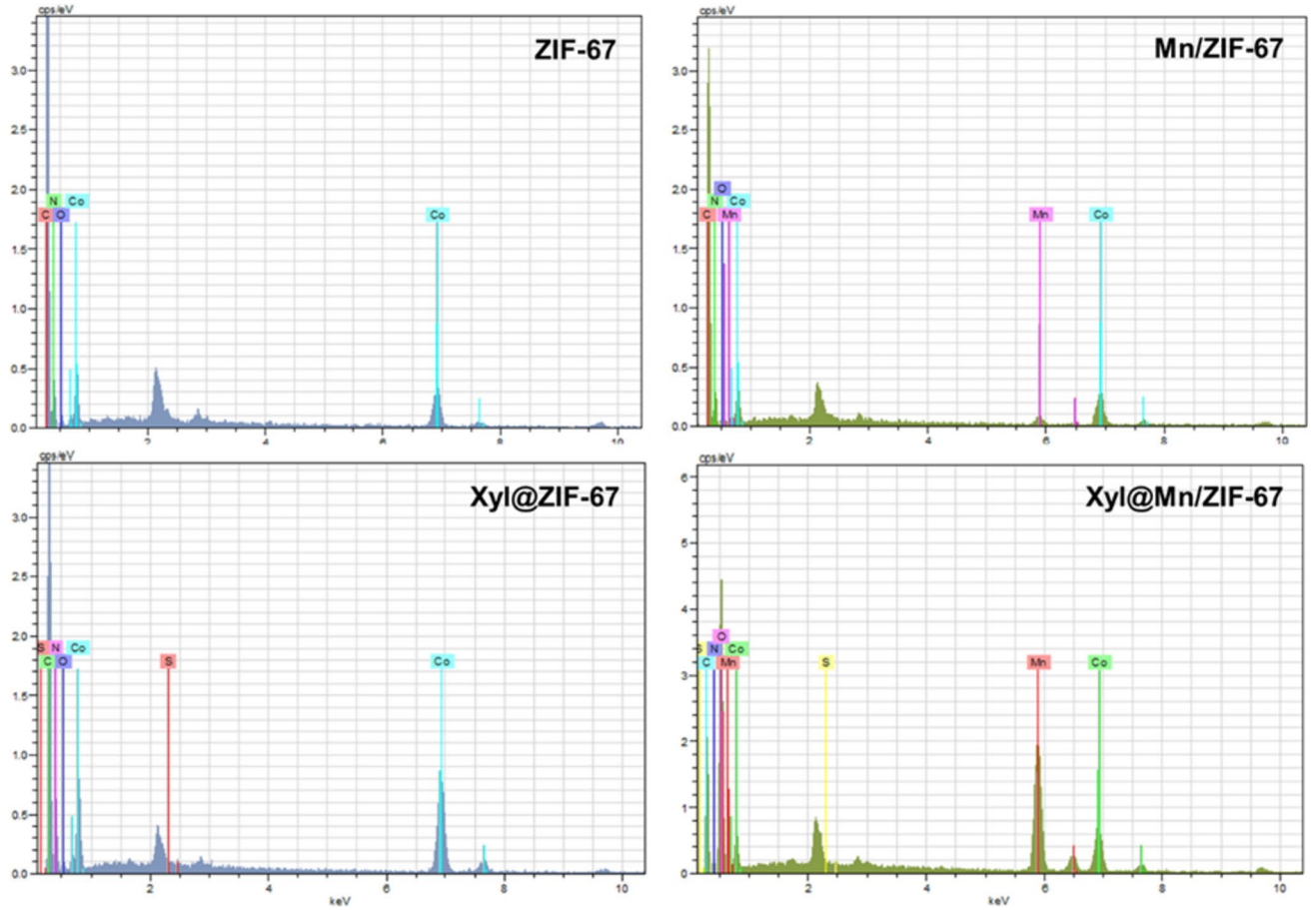

Fig. 7 EDAX patterns of ZIF-67, Mn/ZIF-67, Xyl@ZIF-67, and Xyl@ZIF-67

pH 6.0 whereas Xyl@ZIF-67 and Xyl@Mn/ZIF-67 exhibited maximum activity at pH 8.0 and 7.0, respectively. The shift of the optimum pH for Xyl@ZIF-67 and Xyl@Mn/ZIF-67 to higher values compared to the free Xyl can be explained by the differentiation of pKa values due to the change in ionizable groups. In addition, Xyl@ZIF-67 and Xyl@Mn/ZIF-67 have an activity of over 55% over a wide pH range (5.0, 6.0, 7.0, 8.0, 9.0, and 10.0). Especially, under alkaline conditions, Xyl@ZIF-67 and Xyl@Mn/ZIF-67 were better adapted to alkaline conditions and showed higher activity compared to the free enzyme. This shows that the immobilization process has given Xyl enzyme a high resistance and stability against alkaline conditions. Rafiei et al. encapsulated the lipase enzyme into ZIF-67 and explained that the immobilized lipase has higher activity in the alkaline region than the free lipase as an advantage of the encapsulation method [49]. These outcomes show that our results are in agreement with the literature.

Arrhenius plots were provided for the identification of E_a of free Xyl, Xyl@ZIF-67, and Xyl@Mn/ZIF-67 (Fig. 9). The E_a values of free Xyl, Xyl@ZIF-67, and Xyl@Mn/ZIF-67 were calculated as 11.54, 10.69, and 8.46 kJ/mol, respectively. These values represent a 1.08-fold decrease in E_a for Xyl@ZIF-67 and a 1.36-fold decrease for Xyl@Mn/ZIF-67 relative to the free Xyl. A similar observation was also reported by Amaro-Reyes et al. when Xyl from *Trichoderma longibrachiatum* was immobilized by covalent bonding on magnetic chitosan support [54]. According to Amaro-Reyes et al. [54], the values of E_a were calculated as 45.9 kJ/mol for free Xyl and 13.9 kJ/mol for immobilized Xyl. In another study, the E_a for free and immobilized Xyl diminished from 150.1 to 78.8 kJ/mol [55]. E_a indicates the energy that must be exceeded to convert the substrate into a product. This decrease in E_a observed for immobilized enzymes means that the enzyme has to cross a lower energy barrier to form a transition state complex with its substrate for hydrolysis to products compared to its free form [56, 57]. Thus, the immobilization process provides an energy saving advantage, which makes the enzyme more economically valuable for industrial uses [57]. On the other hand, the decrease in E_a also indicates a lower sensitivity to temperature and a higher stability for the active site of the immobilized enzyme [56, 57].

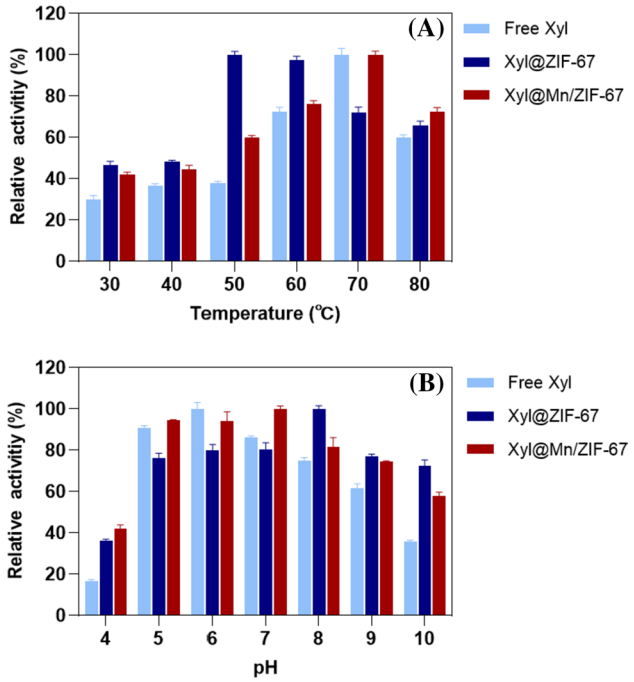

Fig. 8 The effect of different temperature (**A**) and pH (**B**) values on the activity of free Xyl, Xyl@ZIF-67, and Xyl@Mn/ZIF-67

As another significant parameter, Q_{10} (temperature coefficient) was estimated using the E_a value. The Q_{10} values for the free Xyl, Xyl@ZIF-67, and Xyl@Mn/ZIF-67 at their optimal temperatures were found to be 1.09, 1.09, and 1.07, respectively. Typically, the Q_{10} for enzymes ranges from 1 to 2 [58]. The deviation from the Q_{10} value shows that reactions are not temperature dependent (other assay factors participate in controlling the reaction rate than temperature). This result is consistent with that reported by Glekas et al. [35].

3.2.2 Kinetic Parameters

To determine the kinetic parameters of free Xyl, Xyl@ZIF-67, and Xyl@Mn/ZIF-67, the V_{max} and K_m values were attained by the Michaelis−Menten equation using the Lineweaver–Burk plots (Fig. 10) and listed in Table 2. The V_{max} values were estimated as 0.167 ± 0.006, 0.226 ± 0.026, and 0.062 ± 0.003 µmol/min/mL for free Xyl, Xyl@ZIF-67, and Xyl@Mn/ZIF-67, respectively. The K_m values of free Xyl, Xyl@ZIF-67, and Xyl@Mn/ZIF-67 were 3.139 ± 0.049, 5.430 ± 0.161, and 0.799 ± 0.078 mg/mL, respectively. The changes in the kinetic parameters are related to the type of support. For example, the V_{max} value of the Xyl@ZIF-67 was 1.35 times higher than that of the free Xyl, while the V_{max} value of the Xyl@Mn/ZIF-67 diminished 2.69 times.

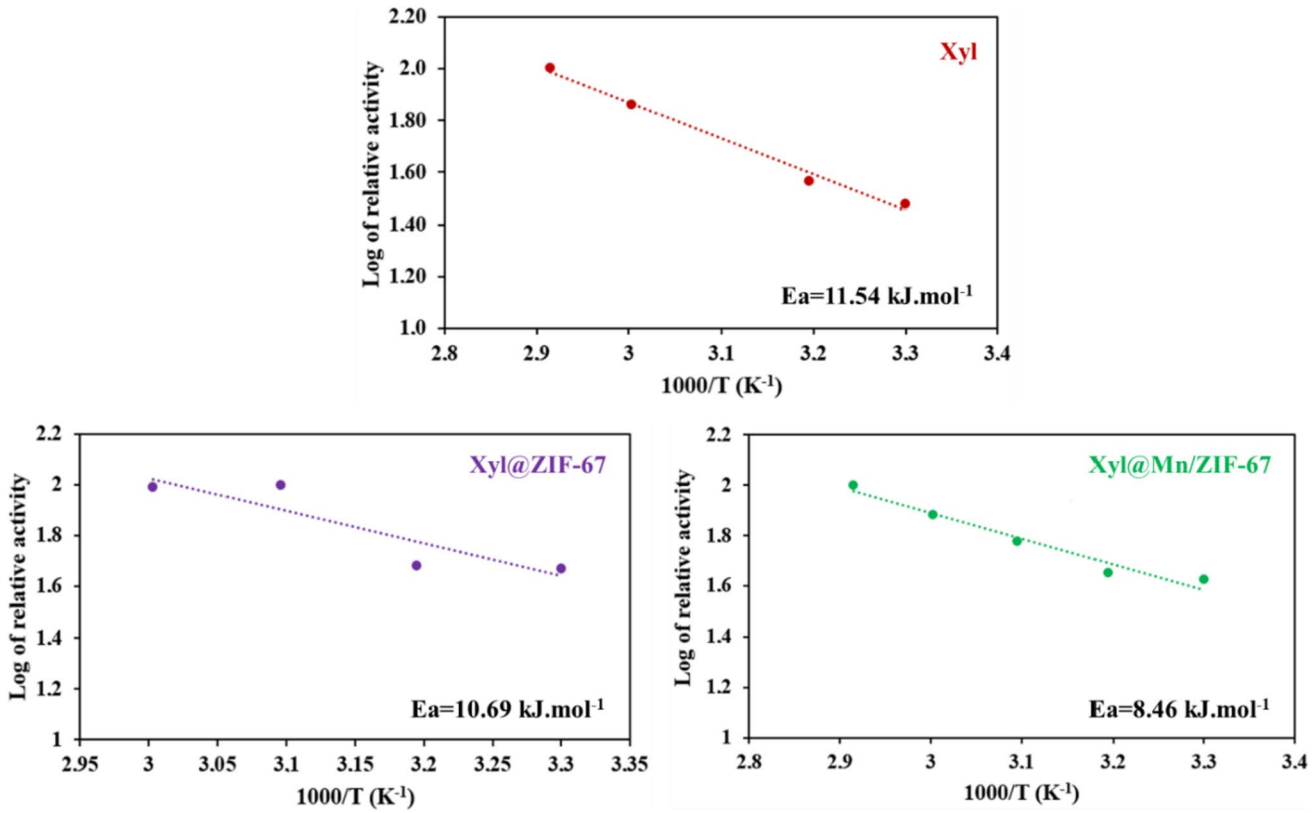

Fig. 9 Arrhenius plots for calculating E_a of free Xyl, Xyl@ZIF-67, and Xyl@Mn/ZIF-67

Table 2 Kinetic parameters and correlation coefficients of free Xyl, Xyl@ZIF-67, and Xyl@Mn/ZIF-67

Enzyme	V_{max} (μmol/min/mL)	K_m (mg/mL)	R^2
Free Xyl	0.167 ± 0.006	3.139 ± 0.049	0.9928
Xyl@ZIF-67	0.226 ± 0.026	5.430 ± 0.161	0.9969
Xyl@Mn/ZIF-67	0.062 ± 0.003	0.799 ± 0.078	0.9928

Similarly, the K_m value of the Xyl@ZIF-67 was 1.73 times higher than that of the free Xyl, while the K_m value of the Xyl@Mn/ZIF-67 reduced 6.79 times. The desired change in the kinetic parameters after immobilization is an increase in the V_{max} value as opposed to a decrease in the K_m value. As discussed before [59], it is well known that conformational, steric, and mass transfer effects resulting from the molecular orientation of the enzyme, as well as microenvironment and cleavage effects, are responsible for the changes in kinetic parameters after immobilization. Additionally, for Xyl@Mn/ZIF-67, the reduction increased the activity of the enzyme, possibly due to the effect of doping Mn ions to the ZIF-67 supports, and allowed the enzyme to interact more easily with the substrate due to the porosity structure [60].

3.2.3 Investigation of Thermal Stability

The free Xyl, Xyl@ZIF-67, and Xyl@Mn/ZIF-67 were incubated at high temperatures (50 °C, 60 °C, and 70 °C) for varying times to investigate the thermal stability of enzyme samples. The results of thermal stability were shown in Fig. 11. It was found that the Xyl@ZIF-67 and Xyl@Mn/ZIF-67 exhibited promising performance. However, with the increase of treatment time at high temperatures, relative activities decreased due to partial thermal inactivation of the enzyme samples. The activity of the free Xyl decreased dramatically after 120 min of thermal treatment at 70 °C. Although the Xyl@ZIF-67 and Xyl@Mn/ZIF-67 show a loss of activity under the same conditions, their activities were definitely higher than their free counterpart. After incubation at 70 °C for 120 min, the free Xyl remained at 28.7% of the activity, while the Xyl@ZIF-67 and Xyl@Mn/ZIF-67 remained at 85.7% and 40.0%, respectively. This excellent thermal stability may be due to the protective effect of ZIF-67, which made Xyl in a more suitable microenvironment and improved its stability. It was also assumed that the thermal activity of the immobilized enzyme obviously depends on the type and properties of the carrier support.

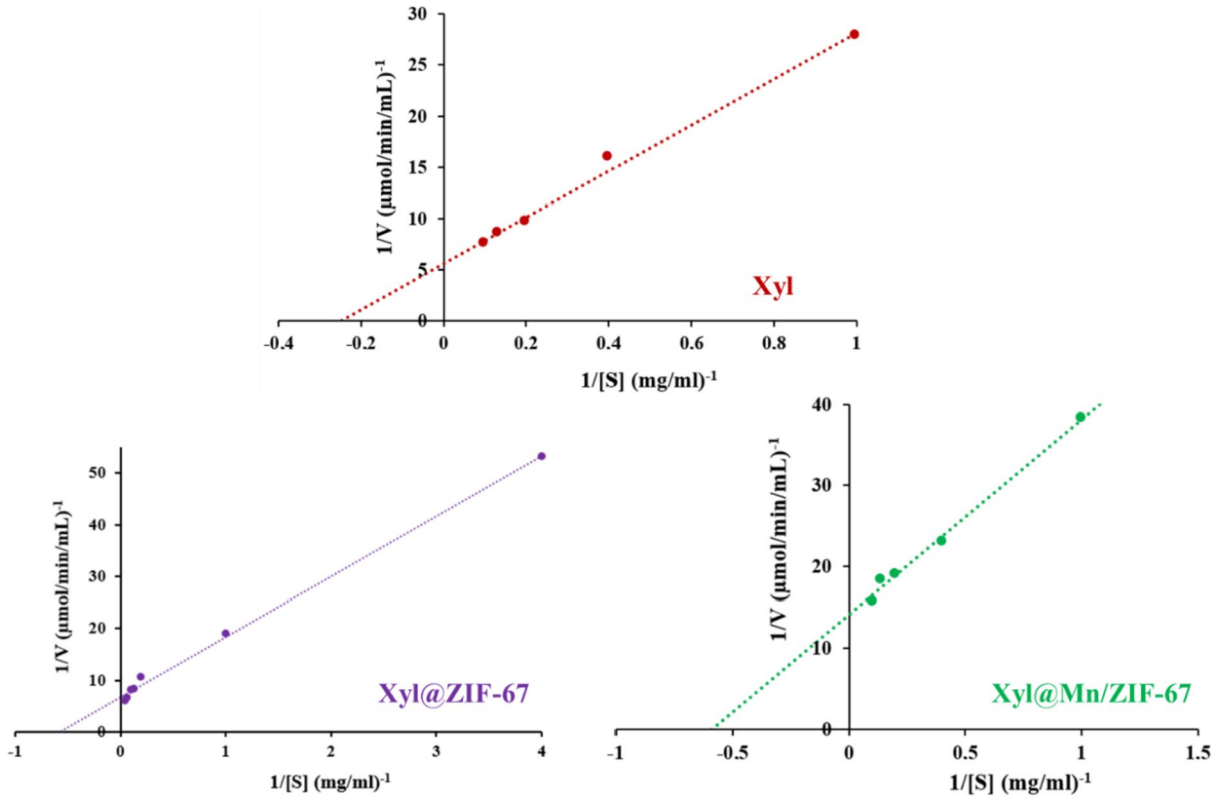

Fig. 10 Lineweaver–Burk plots of free Xyl, Xyl@ZIF-67, and Xyl@Mn/ZIF-67

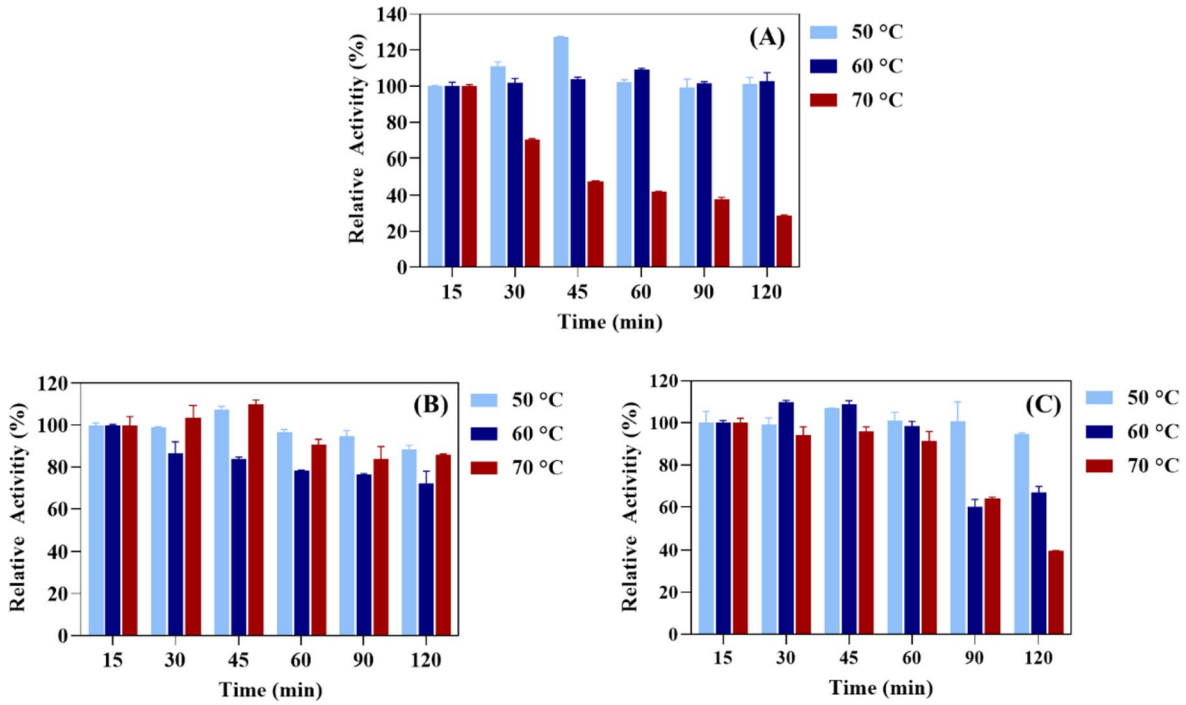

Fig. 11 Thermal stability of **A** free Xyl, **B** Xyl@ZIF-67, and **C** Xyl@Mn/ZIF-67 incubated at 50 °C, 60 and 70 °C

3.2.4 Reusability

Another limitation in the industrial application of free enzymes is that they cannot be reused, as free enzymes cannot be recovered after use [61]. However, the immobilization strategy allows enzymes to be reused in repeated reactions. In the present study, the reusability of the Xyl@ZIF-67 and Xyl@Mn/ZIF-67 was evaluated by repeated use for 8 cycles. As shown in Fig. 12, the Xyl@ZIF-67 and Xyl@Mn/ZIF-67 retained more than 70% of their initial activity after 8 reuses, indicating that both immobilized enzymes have appropriate stability and can be reused. The decrease in the relative hydrolysis efficiency of xylan after 8 catalytic cycles may be due to the blocking of the active centers of the immobilized enzymes by the reaction products. On the other hand, it can also be caused by the leaching of the enzyme from the support material during repeated use [62]. One important conclusion was that Xyl@Mn/ZIF-67 had higher activity compared to Xyl@ZIF-67. This is in line with previous findings and supports our hypothesis.

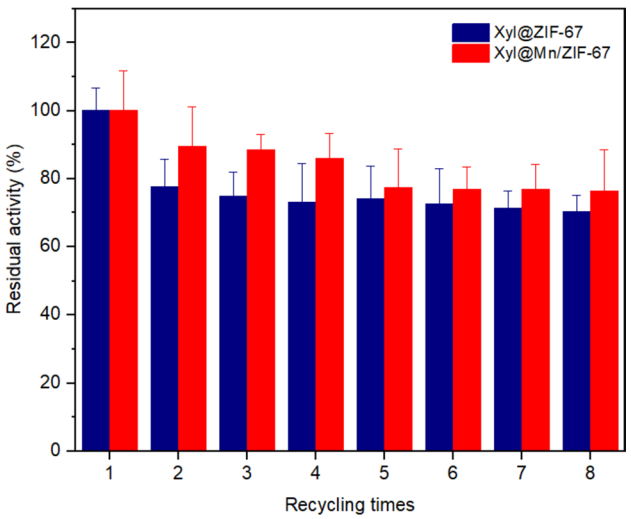

Fig. 12 The reusability profile of the Xyl@ZIF-67 and Xyl@Mn/ZIF-67

3.2.5 Effect of Immobilized Enzyme on Clarification of Apple Juice

Pectin, starch, and hemicellulosic components in juices are the main factors in the formation of turbidity in juice. This turbidity, on the other hand, reduces the demand for consumption and creates difficulties in industrial pasteurization and concentration stages. Removal of these opacity factors can be achieved by appropriate enzymes to produce high quality clarified juices. In this study, the potential of the Xyl@ZIF-67 and Xyl@Mn/ZIF-67 was assessed in clarification of the juice obtained from apple pulps with 81.25% yield. The ability of Xyl@ZIF-67 and Xyl@Mn/ZIF-67 on the clarification of apple juice is shown in Fig. 13. After 60 min of treatment, the Xyl@ZIF-67 and Xyl@Mn/ZIF-67

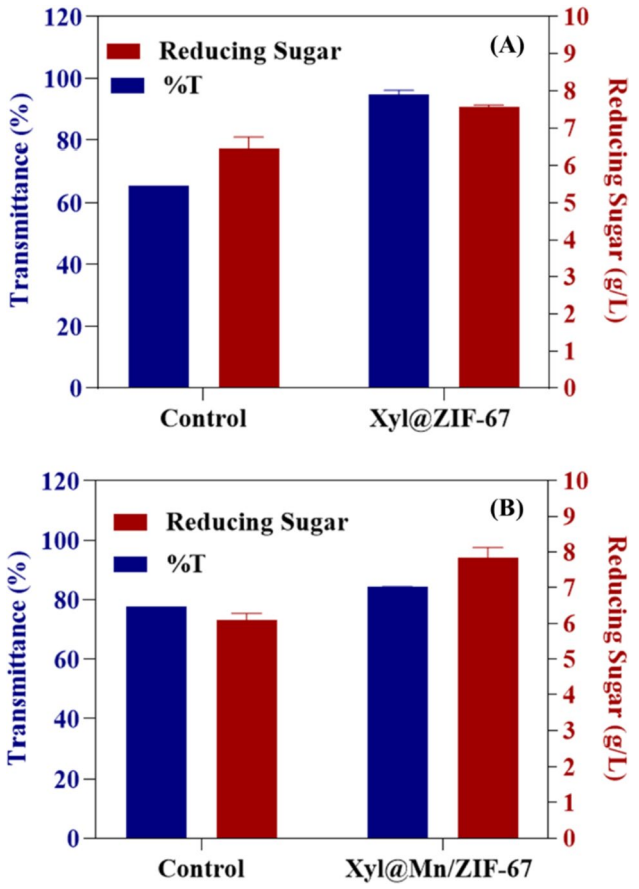

Fig. 13 The effect of Xyl@ZIF-67 (**A**) and Xyl@Mn/ZIF-67 (**B**) on apple juice clarification in terms of transmittance and reducing sugar

were increased transmittance of apple juice from 65.61 to 94.73%, from 77.80 to 84.13%, respectively, when compared to the control. In addition, the reducing sugar amounts of Xyl@ZIF-67 and Xyl@Mn/ZIF-67 increased from 6.45 to 7.55 g/L and 6.03 to 7.83 g/L, respectively (Fig. 13A, B). Processing fruit juices with the Xyl enzyme increases the release of reducing sugar. The reducing sugars released are indicative of the breakdown of hemicellulosic components in the juice. Similar studies in the literature support the increase in the amount of reducing sugar at the end of the clarification process [38, 63]. This study revealed that immobilization of the Xyl into ZIF-67 and Mn/ZIF-67 not only improved stability and reusability of Xyl but also clarified juices quite efficiently.

4 Conclusion

In this study, a viable strategy combined with an appropriate immobilization matrix was investigated to make the Xyl enzyme more stable and effective in industrial scale processes such as juice clarification. Herein, to the best of our knowledge, we have shown that two different carrier supports, ZIF-67 and Mn/ZIF-67, which have not been suggested before in the literature, can be used for Xyl immobilization. For this purpose, the formation of the ZIF-67 and Mn/ZIF-67structures with and without Xyl was carried out by in situ method and these structures were elucidated by structural and morphological characterization processes such as UV–Vis, FT-IR, XRD, SEM, and EDAX. In terms of biochemical characterization, changes were observed in the optimum pH and temperature of the immobilized enzymes compared to the free enzyme. Considering the optimum pH results, it is seen that immobilized enzymes improve the activity considerably at alkaline pHs where free Xyl has low activity. Compared to free Xyl, the K_m value increased for Xyl@ZIF-67 and decreased for Xyl@Mn/ZIF-67. In contrast, the V_{max} value for Xyl@ZIF-67 increased relative to free Xyl and decreased for Xyl@Mn/ZIF-67. Moreover, the Xyl@ZIF-67 and Xyl@Mn/ZIF-67 had more temperature tolerance and excellent reusability. The Xyl@ZIF-67 and Xyl@Mn/ZIF-67 presented high residual activity ($\geq$ 70%) after 8 cycles of reuse. Most importantly, the effect of immobilization of commercially important free Xyl on two different carrier supports on apple juice clarification was investigated. Accordingly, Xyl@ZIF-67 and Xyl@Mn/ZIF-67 increased the clarity of apple juice by 29.12% and 6.33%, respectively. It was observed that the amount of reducing sugar, which is known to be associated with the clarification process, increased at the end of this process. Considering the growing popularity of ZIFs in the MOF class in enzyme immobilization, this study pioneered the rapid and easy synthesis of ZIF-67 structures and their use as a carrier support in immobilization. Meanwhile, this investigation may provide a satisfactory carrier matrix to apply in the industrial production of apple juice.

Acknowledgements This work was partially financed by the Scientific Research Projects Unit of İnönü University (Project Number: FBG-2021-2731). Büşra Bakar is a 100/2000 the Council of Higher Education PhD Scholar Biomaterial and Tissue Engineering subdivision.

Funding Open access funding provided by the Scientific and Technological Research Council of Türkiye (TÜBİTAK).

Declarations

Competing interest The authors express report no declarations of interest.

References

1. Sun Y, Zheng L, Yang Y et al (2020) Metal–organic framework nanocarriers for drug delivery in biomedical applications. Nanomicro Lett 12:103
2. Sun D, Yang D, Wei P et al (2020) One-step electrodeposition of silver nanostructures on 2D/3D metal-organic framework ZIF-67: comparison and application in electrochemical detection of hydrogen peroxide. ACS Appl Mater Interfaces 12:41960–41968
3. Das MC, Xiang S, Zhang Z, Chen B (2011) Functional mixed metal–organic frameworks with metalloligands. Angew Chem Int Ed 50:10510–10520
4. Rowsell JLC, Yaghi OM (2004) Metal–organic frameworks: a new class of porous materials. Microporous Mesoporous Mater 73:3–14
5. Noh K, Lee J, Kim J (2018) Compositions and structures of zeolitic imidazolate frameworks. Isr J Chem 58:1075–1088
6. Zhang C, Dai Y, Johnson JR et al (2012) High performance ZIF-8/6FDA-DAM mixed matrix membrane for propylene/propane separations. J Memb Sci 389:34–42
7. Liang K, Coghlan CJ, Bell SG et al (2015) Enzyme encapsulation in zeolitic imidazolate frameworks: a comparison between controlled co-precipitation and biomimetic mineralisation. Chem Commun 52:473–476
8. Chen G, Huang S, Kou X et al (2019) A convenient and versatile amino-acid-boosted biomimetic strategy for the nondestructive encapsulation of biomacromolecules within metal–organic frameworks. Angew Chem Int Ed 58:1463–1467
9. Liang K, Ricco R, Doherty CM et al (2015) Biomimetic mineralization of metal-organic frameworks as protective coatings for biomacromolecules. Nat Commun 6:7240
10. Kaushal J, Arya SK, Khatri M et al (2022) Efficacious bioconversion of waste walnut shells to xylotetrose and xylopentose by free xylanase (Xy) and MOF immobilized xylanase (Xy-Cu-BTC). Bioresour Technol 357:127374
11. Mehnati-Najafabadi V, Taheri-Kafrani A, Bordbar AK (2018) Xylanase immobilization on modified superparamagnetic graphene oxide nanocomposite: Effect of PEGylation on activity and stability. Int J Biol Macromol 107:418–425
12. Romero-Fernández M, Moreno-Perez S, Orrego H A, et al (2018) Designing continuous flow reaction of xylan hydrolysis for xylooligosaccharides production in packed-bed reactors using xylanase immobilized on methacrylic polymer-based supports. Bioresour Technol 266:249–258
13. Liao H, Ying W, Li X et al (2022) Optimized production of xylooligosaccharides from poplar: a biorefinery strategy with sequential acetic acid/sodium acetate hydrolysis followed by xylanase hydrolysis. Bioresour Technol 347:126683
14. Gufe C, Ngenyoung A, Rattanarojpong T, Khunrae P (2022) Investigation into the effects of CbXyn10C and Xyn11A on xylooligosaccharide profiles produced from sugarcane bagasse and rice straw and their impact on probiotic growth. Bioresour Technol 344:126319
15. Liu J, Li X, Song F et al (2022) Dietary supplementation with low-dose xylooligosaccharide promotes the anti-*salmonella* activity of probiotic *Lactiplantibacillus plantarum* ZS2058 in a murine model. Food Res Int 151:110858
16. Boonchuay P, Wongpoomchai R, Jaturasitha S et al (2021) Prebiotic properties, antioxidant activity, and acute oral toxicity of xylooligosaccharides derived enzymatically from corncob. Food Biosci 40:100895
17. Singh AK, Mishra B, Bedford MR, Jha R (2021) Effects of supplemental xylanase and xylooligosaccharides on production performance and gut health variables of broiler chickens. J Anim Sci Biotechnol 12:98
18. Le B, Ngoc APT, Yang SH (2020) Synbiotic fermented soymilk with *Weissella cibaria* FB069 and xylooligosaccharides prevents proliferation in human colon cancer cells. J Appl Microbiol 128:1486–1496
19. Shahrestani H, Taheri-Kafrani A, Soozanipour A, Tavakoli O (2016) Enzymatic clarification of fruit juices using xylanase immobilized on 1,3,5-triazine-functionalized silica-encapsulated magnetic nanoparticles. Biochem Eng J 109:51–58
20. Nørgaard JV, Pedersen TF, Blaabjerg K et al (2016) Xylanase supplementation to rye diets for growing pigs. J Anim Sci 94:91–94
21. Woolridge EM (2014) Mixed enzyme systems for delignification of lignocellulosic biomass. Catalysts 4:1–35
22. Rosmine E, Sainjan NC, Silvester R et al (2017) Statistical optimisation of xylanase production by estuarine *Streptomyces* sp. and its application in clarification of fruit juice. J Genet Eng Biotechnol 15:393–401
23. Kaushal J, Khatri M, Singh G, Arya SK (2021) A multifaceted enzyme conspicuous in fruit juice clarification: an elaborate review on xylanase. Int J Biol Macromol 193:1350–1361
24. Wang Y, Zhan W, Chen Z et al (2020) Advanced 3D hollow-out ZnZrO@C combined with hierarchical zeolite for highly active and selective CO hydrogenation to aromatics. ACS Catal 10:7177–7187
25. Wang L, Liu G, Ren Y et al (2020) Integrating target-triggered aptamer-capped HRP@metal-organic frameworks with a colorimeter readout for on-site sensitive detection of antibiotics. Anal Chem 92:14259–14266
26. Chen H, Liu L, Lv S et al (2010) Immobilization of *Aspergillus niger* xylanase on chitosan using dialdehyde starch as a coupling agent. Appl Biochem Biotechnol 162:24–32
27. Coutinho TC, Tardioli PW, Farinas CS (2020) Hydroxyapatite nanoparticles modified with metal ions for xylanase immobilization. Int J Biol Macromol 150:344–353
28. Kumar A, Patel SKS, Mardan B et al (2018) Immobilization of xylanase using a protein-inorganic hybrid system. J Microbiol Biotechnol 28:638–644
29. Álvarez-Cervantes J, Hernández-Domínguez EM, Arana-Cuenca A et al (2013) Purification and characterization of xylanase SRXL1 from *Sporisorium reilianum* grown in submerged and solid-state fermentation. BioRes 8:5309–5318
30. Adigüzel AO, Tunçer M (2016) Production, characterization and application of a xylanase from *Streptomyces* sp. AOA40 in fruit juice and bakery industries. Food Biotechnol 30:189–218
31. Guo C, Guo J, Zhang Y et al (2018) Synthesis of core–shell ZIF-67@Co-MOF-74 catalyst with controllable shell thickness and enhanced photocatalytic activity for visible light-driven water oxidation. CrystEngComm 20:7659–7665
32. Lourenço AA, Silva VD, da Silva RB et al (2021) Metal-organic frameworks as template for synthesis of Mn^{3+}/Mn^{4+} mixed valence manganese cobaltites electrocatalysts for oxygen evolution reaction. J Colloid Interface Sci 582:124–136
33. Bailey MJ, Biely P, Poutanen K (1992) Interlaboratory testing of methods for assay of xylanase activity. J Biotechnol 23:257–270
34. Noma SAA, Acet Ö, Ulu A et al (2020) L-Asparaginase immobilized p(HEMA-GMA) cryogels: a recent study for biochemical, thermodynamic and kinetic parameters. Polym Test 93:106980

35. Glekas PD, Kalantzi S, Dalios A et al (2022) Biochemical and thermodynamic studies on a novel thermotolerant GH10 xylanase from *Bacillus safensis*. Biomolecules 12:790
36. Alagöz D, Varan NE, Toprak A et al (2022) Immobilization of xylanase on differently functionalized silica gel supports for orange juice clarification. Process Biochem 113:270–280
37. Ozyilmaz G, Gunay E (2023) Clarification of apple, grape and pear juices by co-immobilized amylase, pectinase and cellulase. Food Chem 398:133900
38. Haile S, Masi C, Tafesse M (2022) Isolation and characterization of pectinase-producing bacteria (*Serratia marcescens*) from avocado peel waste for juice clarification. BMC Microbiol 22:145
39. Saeedi M, Fazaeli R, Aliyan H (2016) Nanostructured sodium–zeolite imidazolate framework (ZIF-8) doped with potassium by sol–gel processing for biodiesel production from soybean oil. J Solgel Sci Technol 77:404–415
40. Zhou K, Mousavi B, Luo Z et al (2017) Characterization and properties of Zn/Co zeolitic imidazolate frameworks vs. ZIF-8 and ZIF-67. J Mater Chem A Mater 5:952–957
41. Ediati R, Elfianuar P, Santoso E et al (2019) Synthesis of MCM-41/ZIF-67 composite for enhanced adsorptive removal of methyl orange in aqueous solution. In: Krishnappa M (ed) Mesoporous materials - properties and applications. IntechOpen. https://doi.org/10.5772/intechopen.84691
42. dos Santos JP, Zavareze E, da Dias R, Vanier ARG NL (2018) Immobilization of xylanase and xylanase–β-cyclodextrin complex in polyvinyl alcohol via electrospinning improves enzyme activity at a wide pH and temperature range. Int J Biol Macromol 118:1676–1684
43. Wang G, Liu J, Yue F et al (2022) Dual enzyme electrochemiluminescence sensor based on in situ synthesis of ZIF-67@AgNPs for the detection of IMP in fresh meat. LWT 165:113658
44. Xu H, Fu N, Zheng J et al (2022) Mn-doped bimetallic synergistic catalysis boosts for enzymatic phosphorylation of N-acetylglucosamine/ N-acetylgalactosamine and their derivatives. Bioorg Chem 128:106041
45. Öztürk Z, Hofmann JP, Lutz M et al (2015) Controlled synthesis of phase-pure zeolitic imidazolate framework Co-ZIF-9. Eur J Inorg Chem 2015:1625–1630
46. Abdelhameed RM, El-Shahat M (2019) Fabrication of ZIF-67@MIL-125-NH_2 nanocomposite with enhanced visible light photoreduction activity. J Environ Chem Eng 7:103194
47. Kahoush M, Behary N, Guan J et al (2021) Genipin-mediated immobilization of glucose oxidase enzyme on carbon felt for use as heterogeneous catalyst in sustainable wastewater treatment. J Environ Chem Eng 9:105633
48. Liu X, Chen W, Lian M et al (2019) Enzyme immobilization on ZIF-67/MWCNT composite engenders high sensitivity electrochemical sensing. J Electroanal Chem 833:505–511
49. Rafiei S, Tangestaninejad S, Horcajada P et al (2018) Efficient biodiesel production using a lipase@ZIF-67 nanobioreactor. Chem Eng J 334:1233–1241
50. Ulu A (2020) Metal–organic frameworks (MOFs): a novel support platform for ASNase immobilization. J Mater Sci 55:6130–6144
51. Deng Y, Dong Y, Wang G et al (2017) Well-defined ZIF-Derived Fe–N codoped carbon nanoframes as efficient oxygen reduction catalysts. ACS Appl Mater Interfaces 9:9699–9709
52. Hafızosmanoğlu G, Ulu A, Köytepe S, Ateş B (2024) Fabrication of oleic acid grafted starch-based hybrid carriers for L-asparaginase encapsulation. Starch Stärke 76:2100152
53. Jankowska K, Zdarta J, Grzywaczyk A et al (2020) Electrospun poly(methyl methacrylate)/polyaniline fibres as a support for laccase immobilisation and use in dye decolourisation. Environ Res 184:109332
54. Amaro-Reyes A, Díaz-Hernández A, Gracida J et al (2019) Enhanced performance of immobilized xylanase/filter paper-ase on a magnetic chitosan support. Catalysts 9:966
55. Gupta G, Sahai V, Gupta RK (2014) Thermal stability and thermodynamics of xylanase from *Melanocarpus albomyces* in presence of polyols and salts. BioRes 9:5801–5816
56. Amin F, Asad SA, Nazli Z et al (2023) Immobilization, biochemical, thermodynamic, and fruit juice clarification properties of lignocellulosic biomass-derived exo-polygalacturonase from *Penicillium paxilli*. Biomass Convers Biorefin 13:13181–13196
57. Sadaqat B, Sha C, Dar MA et al (2022) Modifying thermostability and reusability of hyperthermophilic mannanase by immobilization on glutaraldehyde cross-linked chitosan beads. Biomolecules 12:999
58. Singh AK, Chhatpar HS (2011) Purification and characterization of chitinase from *Paenibacillus* sp. D1. Appl Biochem Biotechnol 164:77–88
59. Cabrera MP, da Fonseca TF, de Souza RVB et al (2018) Polyaniline-coated magnetic diatomite nanoparticles as a matrix for immobilizing enzymes. Appl Surf Sci 457:21–29
60. Yuan L, Chai J, Wang S et al (2023) Biomimetic laccase-Cu_2O@MOF for synergetic degradation and colorimetric detection of phenolic compounds in wastewater. Environ Technol Innov 30:103085
61. Cheng Z, Sun Z, Wei F et al (2023) Immobilization of the crude enzyme extracted from *Stenotrophomonas* sp. GYH within modified zeolitic imidazolate framework (ZIF-8.NH_2) and its application in trichloromethane removal. Environ Funct Mater 2:36–45
62. Jankowska K, Su Z, Sigurdardóttir SB et al (2021) Tailor-made novel electrospun polystyrene/poly(D,L-lactide-co-glycolide) for oxidoreductases immobilization: improvement of catalytic properties under extreme reaction conditions. Bioorg Chem 114:105036
63. Cakmak U, Saglam Ertunga N (2016) Gene cloning, expression, immobilization and characterization of endo-xylanase from *Geobacillus* sp. TF16 and investigation of its industrial applications. J Mol Catal B Enzym 133:S288–S298